

# *LISA* and *LISA PathFinder*, the endeavour to detect low frequency GWs

H Araújo<sup>1</sup>, C Boatella<sup>2</sup>, M Chmeissani<sup>3</sup>, A Conchillo<sup>2</sup>, E García-Berro<sup>2,4</sup>, C Grimani<sup>5</sup>, W Hajdas<sup>6</sup>, A Lobo<sup>2,7,10</sup>, Ll Martínez<sup>8</sup>, M Nofrarias<sup>2</sup>, JA Ortega<sup>2</sup>, C Puigdemgols<sup>3</sup>, J Ramos-Castro<sup>9</sup>, J Sanjuán<sup>2</sup>, P Wass<sup>1</sup> and X Xirgu<sup>2</sup>

<sup>1</sup> Blackett Laboratory, Imperial College London, Prince Consort Road, London SW7 2BW, UK

<sup>2</sup> Institut d'Estudis Espacials de Catalunya (*IEEC*), Edifici Nexus, Gran Capità 2-4, 08034 Barcelona, Spain

<sup>3</sup> Institut de Física d'Altes Energies (*IFAE*), Edifici C, Universitat Autònoma de Barcelona, 08193 Bellaterra, (Barcelona), Spain

<sup>4</sup> Departament de Física Aplicada, Universitat Politècnica de Catalunya, Escola Politècnica Superior de Castelldefels, Avda. Canal Olímpic s/n, 08860 Castelldefels, Spain

<sup>5</sup> Università degli Studi di Urbino, and *INFN* Florence, Istituto di Fisica, Via Santa Chiara 27, 61029 Urbino, Italy

<sup>6</sup> Department of Particles and Matter, Paul Scherrer Institut, ODR 120, 5232 Villigen, Switzerland

<sup>7</sup> Institut de Ciències del Espacio, *CSIC*, Campus *UAB*, Facultat de Ciències, Torre C-5 Parell, 2<sup>a</sup> Planta, E-08193 Bellaterra (Cerdanyola del Vallès), Barcelona, Spain

<sup>8</sup> *Atípic*, Parc Tecnològic del Vallès, 08290 Cerdanyola del Vallès, Barcelona, Spain

<sup>9</sup> Departament d'Enginyeria Electrònica, *UPC*, Campus Nord, Edif. C4, Jordi Girona 1-3, 08034 Barcelona, Spain

E-mail: lobo@ieec.fcr.es

**Abstract.** This is a review about *LISA* and its technology demonstrator, *LISAPathFinder*. We first describe the conceptual problems which need to be overcome in order to set up a working interferometric detector of low frequency Gravitational Waves (GW), then summarise the solutions to them as currently conceived by the *LISA* mission team. This will show that some of these solutions require new technological abilities which are still under development, and which need proper test before being fully implemented. *LISAPathFinder* (*LPF*) is the testbed for such technologies. The final part of the paper will address the ideas and concepts behind the *PathFinder* as well as their impact on *LISA*.

## 1. Introduction

Gravitational Waves (GW), i.e., radiant gravitational fields, were absent in Newton's classical theory of gravity. For over two centuries, though, nobody was missing them. It was only with the advent of Einstein's Special Theory of Relativity [1] in the early twentieth century that such absence began to create some distress. It was indeed very odd, it appeared to physicists at that time, that gravitation should *instantly* propagate to even the remotest places in the Universe,

<sup>10</sup> To whom correspondence should be addressed.

since this was blatantly against the principle of causality just born out of the discovery of the limit speed,  $c$  —the speed of light in empty space.

Let us recall Poisson's equation for the gravitational potential:

$$\nabla\phi(\mathbf{x}, t) = 4\pi G \varrho(\mathbf{x}, t) \quad (1)$$

whose formal solution is

$$\phi(\mathbf{x}, t) = -G \int \frac{\varrho(\mathbf{x}', t)}{|\mathbf{x} - \mathbf{x}'|} d^3x' \quad (2)$$

We observe in this formula, relating the gravitational potential  $\phi(\mathbf{x}, t)$  to the density of gravitating matter  $\varrho(\mathbf{x}, t)$ , that there are no differential coefficients involving the time variable  $t$ , which merely plays the role of a *parameter* in the equation. This means that any changes in the source density happening at time  $t = t_0$ , say, are *also* felt at time  $t = t_0$  by the gravitational potential, no matter *where*. In other words, the value of the gravitational potential  $\phi$  varies in time exactly in parallel with the time variations of the generating density  $\varrho$ , and does so for *all* values of the field space coordinate  $\mathbf{x}$ . We thus see that Newton's theory predicts that gravitational perturbations, hence gravitational energy, too, travel across empty space with *infinite speed*.

A very interesting account of the endeavours in pursuit of the solution to the riddle to build a *causal* theory of gravity can be found e.g. in a renowned book by A Pais [2]. Let us simply recall here that Einstein's General theory of Relativity (GR), the usually accepted final solution, predicts that gravitational waves do indeed exist, which travel at the speed of light in otherwise flat empty space, have *two* polarisation degrees of freedom, and are *transverse* to the propagation direction. In a suitable quasi-Lorentzian coordinate system, Einstein's vacuum GW equations read [3]

$$\square \left( h_{\mu\nu} - \frac{1}{2} \eta_{\mu\nu} \eta^{\rho\sigma} h_{\rho\sigma} \right) = 0 \quad (3)$$

where  $h_{\mu\nu}$  are small perturbations to the flat Lorentzian geometry,  $\eta_{\mu\nu}$ :

$$g_{\mu\nu}(\mathbf{x}, t) = \eta_{\mu\nu} + h_{\mu\nu}(\mathbf{x}, t), \quad |h_{\mu\nu}(\mathbf{x}, t)| \ll 1 \quad (4)$$

The relationship between the GW amplitudes and their sources, i.e., the equivalent of equation (2), is also textbook material [4]. In the far zone [5], it is given by the *quadrupole formula*

$$h_{ij}(\mathbf{x}, t) = \frac{4G}{c^4|\mathbf{x}|} \mathcal{P}_{ijkl} \ddot{Q}_{kl}(t - |\mathbf{x}|/c) \quad (5)$$

where  $\mathcal{P}_{ijkl} = \mathcal{P}_{ik}\mathcal{P}_{jl} - (1/2)\mathcal{P}_{ij}\mathcal{P}_{kl}$ , with  $\mathcal{P}_{ij} = \delta_{ij} - x_i x_j / |\mathbf{x}|^2$ , is the *transverse-traceless* (TT) projection operator, and

$$Q_{ij}(t) \equiv \int_{\text{Source}} \left( x_i x_j - \frac{1}{3} |\mathbf{x}|^2 \delta_{ij} \right) \varrho(\mathbf{x}, t) d^3x \quad (6)$$

is the source's quadrupole moment.

Equation (5) reflects the *causal* nature of GWs in the *retarded time* argument in the rhs. For *gravitationally bound* systems, the formula can also be easily used to find an order of magnitude estimate of the amplitude of the GW emission of a given source: for one of mass  $M$  and linear size  $\ell$ , which is observed from a distance  $R$  away, it gives

$$h \sim \frac{\ell}{R} \left( \frac{GM}{\ell c^2} \right)^2 \quad (7)$$

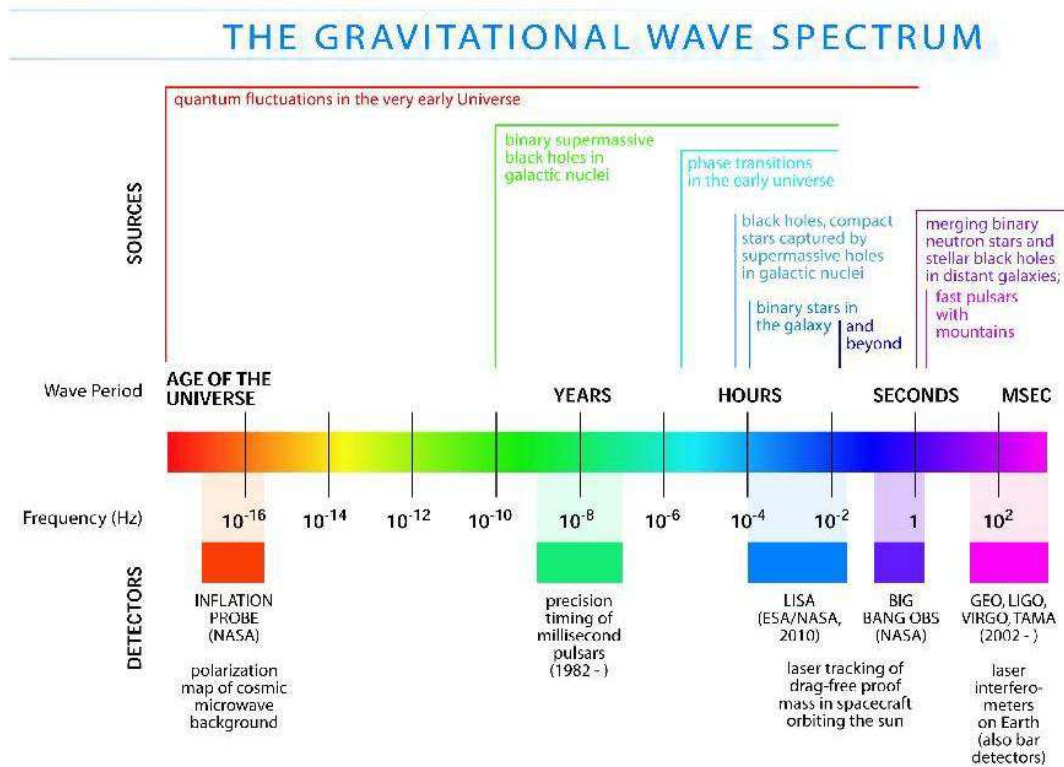


**Figure 1.** The frequency spectrum of GWs.

Note that the term inside the brackets is the ratio between the source's *Schwarzschild radius* and its actual size, while the other term is the ratio between the size of the source and its distance to the observer. The combination of these two factors results in extremely small numbers for GW amplitudes, at most  $\sim 10^{-18}$  in the most favourable conditions of source intensity and likely distance. Any terrestrial, or even Solar System sources conceivable generate much weaker signals. This is most likely the reason why Celestial Mechanics managed to live a long and successful life without GWs in its body of doctrine.

But once we know that GWs *do* exist [6], we discover they can open a whole *new window* for the observation of the Universe, so far naturally unexplored, and with surely unsuspected capabilities in store. The first experimental attempts to detect GWs with a dedicated instrument are almost half a century old, and date back to the early 1960s, when J Weber designed, built and operated two very sensitive cylindrical bars [7].

Weber's claims of GW sightings eventually proved unconvincing, but they did foster new research activity in the field of GW detectors. Current earth based detectors are orders of magnitude more sensitive than Weber's [8, 9], and new concept [10] interferometric antennas have taken over Weber's idea of acoustic sensing in favour of optical techniques. Such detectors as LIGO [11], VIRGO [12] or GEO-600 [13] are in very advanced states of development, and should be shortly generating true GW observatory data.

Earth based detectors share however a common sensitivity limitation, set by unavoidable seismic and gravity gradient noise [14]. These make basically unreachable the frequency band below  $\sim 10$  Hz, with the consequence that low frequency GWs cannot possibly be observed from the earth's surface. If we wish to see such GWs then we have to move out to space, far from terrestrial accidents. This is the reason for *LISA*, the first low frequency GW detector, which should fly in the time frame of 2015 with good sensitivity in the band around 1 mHz [15].

There is a qualitative argument that low frequency GW signals should be more abundant than high frequency ones —where “high frequency” means around and above 1 kHz. This is that large scale mass motions have typically long time scales, too, mostly far from the fraction-of-a-second scale. Figure 1 shows the frequency spectrum of GWs as we currently conceive it, and roughly confirms that qualitative argument. The figure also carries indications of the detectors sensitive in each frequency region: as can be seen, *LISA* clearly covers a wider range of likely GW sources than cover any earth based antennas. This makes of *LISA* a specially attractive project, as it will provide the only means we have to access such very interesting signals. In addition, *LISA*’s potential for discovery of new unforeseen sources is also vigorously there, and it will add to the potential of earth based instruments.

This paper is a review about *LISA* workings, from the mission principles and concept to its technology precursor *LISA* PathFinder (*LPF*). Its organisation follows sequentially these topics.

## 2. *LISA*

As is well known [16], interferometric detection of GWs requires the interferometer arm-length to be close to  $\lambda_{\text{GW}}/2$ . If we aim at GWs of frequencies around 1 mHz, we correspondingly need arm-lengths in the order of several million kilometres. For *LISA* the option taken is

$$\textit{LISA's arm-length} = 5 \times 10^6 \text{ kilometres}$$

The configuration is shown in figure 2: it is a constellation of three spacecraft occupying the vertexes of an equilateral triangle. There are a few important facts about this configuration which we now summarise briefly.

### 2.1. Active mirrors

The 5 million km arm-length poses a problem to classical Michelson interferometry, which is the following: even if the laser beam is collimated to high precision, there is a minimum *beam divergence* which cannot be avoided. For a 1 watt laser, as foreseen for *LISA*, this limit is

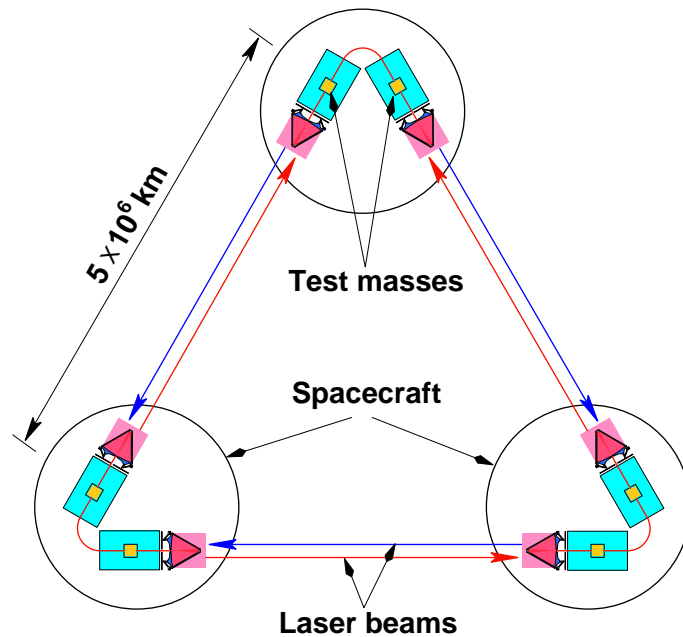
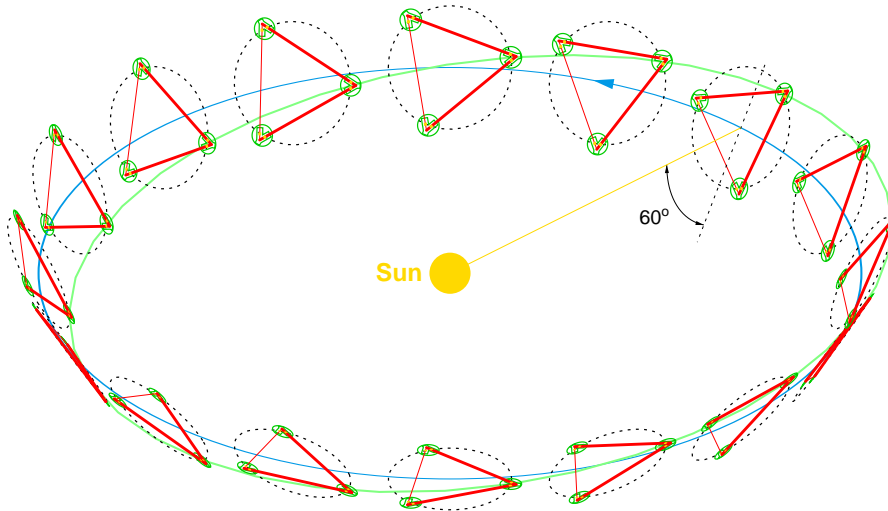


Figure 2. *LISA*’s equilateral triangle configuration.



**Figure 3.** *LISA*'s three spacecraft orbital evolution around the Sun. The centre of the triangle follows the Earth's ecliptic, while the triangle itself rotates clockwise around its centre once per year.

about  $4 \times 10^{-6}$  rad. The consequence of this divergence is that, after 5 million km, the initial small spot of the laser source has become a considerable spot of about 20 km in diameter. . . Therefore only a very small fraction of the emitted light is actually collected by the remote mirror, which is a telescope of only 40 cm in diameter. If light were simply reflected back to the originating source then divergence of the already weakened light beam would result in an extremely degraded power for interferometry, which would actually make it impossible: only a few hundred photons per hour would be received, a figure well below the shot noise in the light sensing electronics (photodiodes).

To avoid this, *active mirrors*, or *transponders* are envisaged. These are devices which, by means of a local oscillator, can capture phase information of the incoming light beam and order the re-emission of the full 1 watt laser with that phase information encoded in it. In this form, interferometry with long arms is made possible.

## 2.2. Orbit

Obviously, there is no way one can possibly lock *LISA*'s interferometer arm-length to 5 million km. In fact, the three spacecraft will be primarily guided by the interplanetary gravitational field, i.e., the field of the Sun and the other solar system bodies.

On the other hand, as we shall shortly see, *LISA* will be required to perform pico-metre interferometry, which means it should be able to detect distance *variations* between pairs of spacecraft to picometre precision. This, in the milli-Hz frequency band.

The question naturally arises whether such measurement precision is compatible with the laws of Celestial Mechanics which govern the motions of the *LISA* spacecraft. Astrometric studies [18, 19] have shown that there exists an optimised satellite configuration, which is displayed in figure 3: the three spacecraft constellation rotates clockwise around its barycentre with a period of one year, while the barycentre follows the ecliptic (blue line in the drawing),  $20^\circ$  behind the Earth —or, equivalently, 45 million km<sup>1</sup>. The plane of the three satellites is

<sup>1</sup> This number is the result of an accepted compromise: if *LISA* is close to the Earth then gravitational perturbations distort its configuration; if *LISA* is far then we may run into telemetry problems.

inclined  $60^\circ$  relative to the ecliptic, and the normal to it correspondingly describes a cone in the sky. *LISA* is thus not pointing to a fixed location. Each of the three spacecraft is in an orbit which is very circular (eccentricity = 0.01), and the plane of each orbit is inclined  $1^\circ$  relative to the ecliptic.

Even though this is basically the most stable orbit, in the sense that it best keeps the triangular shape of the spacecraft constellation, such shape is far from constant: the arm-lengths change, and so do the angles between the arms; consequently, the spacecraft drift back and forth from one another, too. These changes are not negligible, as we see in the examples given in figure 4: arm-length differences undergo peak-to-peak variations of about 120 000 km, and relative velocities can be  $\pm 15$  km/sec. Not shown in the figure, angles between contiguous arms can vary by about 1 degree, peak-to-peak.

The reader may wonder how can one possibly do picometre interferometry in a systems which drifts away by tens of thousands of kilometres. The answer to this is that one is interested in length variations over time scales of hours—which correspond to milli-Hz frequencies. A look at the graphs of figure 4 indicates that orbital changes happen instead in time scales of months, i.e., far from the frequency of the GW signals we are interested in. In addition, short time prediction of astronomical ephemeris—such as happen in the Solar System—is very reliable, and poses therefore no (theoretical) problem for detection.

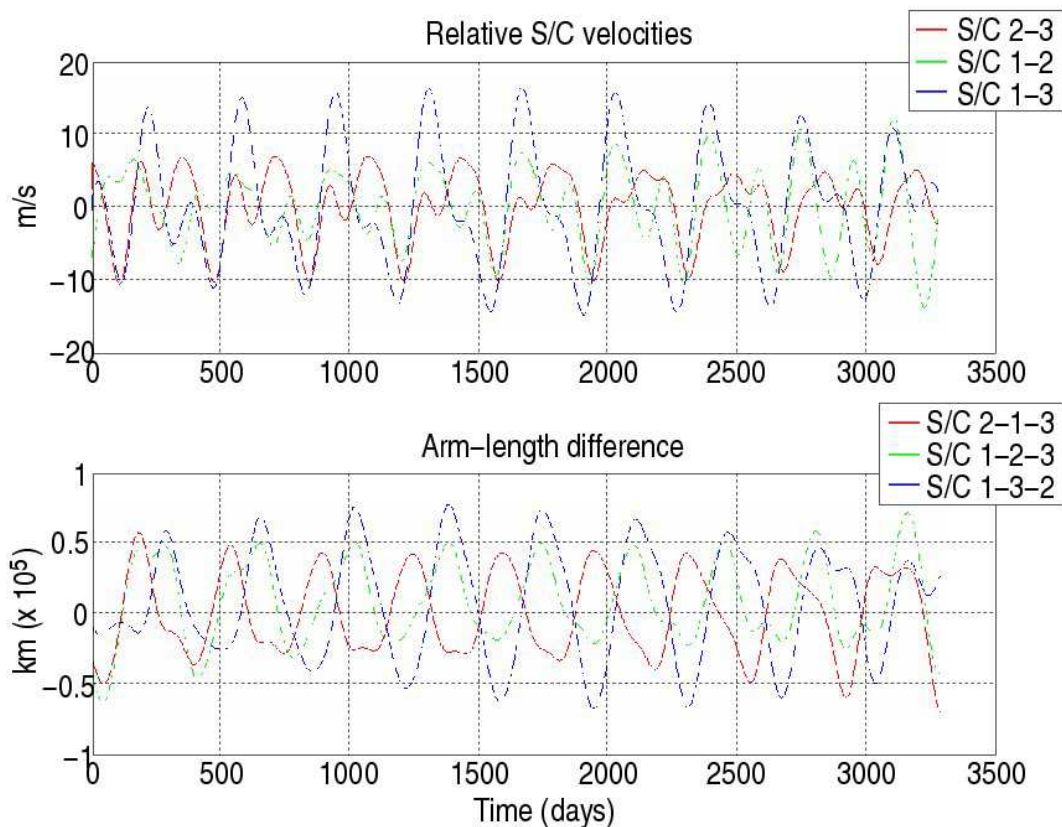


**Figure 4.** Variations in relative velocity between spacecraft and differences between arm-lengths over a period of 10 years, which is *LISA*'s extended lifetime.

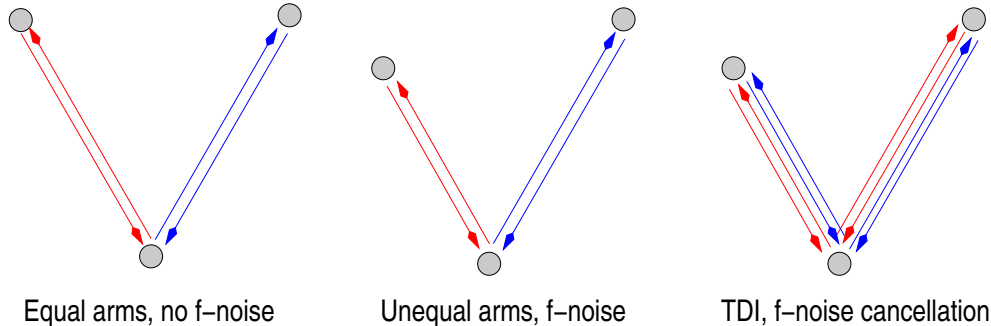


**Figure 5.** Concept of the TDI variable of equation (11): frequency noise is proportional to the difference between the blue and the red beam lengths.

### 2.3. Time delay interferometry

The varying length of the interferometer arms has however a setback of a different nature. This is linked to the influence of *frequency fluctuations* on the readout of the phase meter, where light coming from different arms is recombined to generate an interference pattern.

Traditional, equal arm-length Michelson interferometry does not have this problem: light is generated in a laser source, then divided into two beams at a beam splitter, then sent out to a pair of equally distant mirrors, then reflected back by the latter and recombined again at the beam splitter, then finally the interfering beam analysed by a photo-detector, e.g. a photodiode. A real laser does not have an exact frequency, it actually *fluctuates*. But the fluctuations go undetected by the Michelson scheme: indeed, the interferometer signal in this scheme is the phase *difference* between the two traveling beams, hence any fluctuations mutually cancel if both beams have traveled the same distance from the instant of split-up to that of recombination.

Phase noise thus enters the scenario whenever the optical path of the laser beams differ. The intensity of noise depends on the stability of the laser frequency: if the frequency fluctuates by  $\delta f$  and the arm-length difference is  $\Delta L$ , then the optical path difference  $\delta x$  is readily seen to be given (in first order) by

$$\delta x = \frac{\delta f}{f} \Delta L \quad (8)$$

A very stable infra-red laser ( $\lambda = 1.064 \mu\text{m}$ ) is envisaged for *LISA*, with a phase stability of one part in  $10^{13}$  per square root of Hertz, or  $S_f^{1/2} \simeq 30 \text{ Hz}/\sqrt{\text{Hz}}$ . If we wish to do pico-metre interferometry —see section 3 below— the length variations we can tolerate are, according to formula (8),  $\Delta L < 200$  metres. But, as we have just seen, *LISA* undergoes much larger changes, so we have a problem here.

This is precisely the problem Time Delay Interferometry, or TDI, addresses. TDI is a *post-processing* technique to remove frequency noise from interferometer data. It is therefore not implemented in hardware, but purely in software. An excellent and updated review will be found in [20]. Here we shall only give the simplest example in order to illustrate the concept.

Assume  $\phi(t)$  is the phase of the laser as it enters the beam splitter before the light is distributed to two of the *LISA* arms, which have lengths  $L_1$  and  $L_2$ , respectively. Let  $y_1(t)$  and  $y_2(t)$  be the phase readings at the beam splitter *after* the light has come back from each of the arms. Then

$$y_1(t) = \phi(t - 2L_1/c) - \phi(t) + \chi_1(t) + n_1(t) \quad (9)$$

$$y_2(t) = \phi(t - 2L_2/c) - \phi(t) + \chi_2(t) + n_2(t) \quad (10)$$

where  $\chi_1(t)$ ,  $\chi_2(t)$  are GW phase shifts, and  $n_1(t)$ ,  $n_2(t)$  are other noise contributions, not due

to frequency random jitter. This latter term is included in  $\phi(t)$ . The following TDI variable can now be defined:

$$X(t) = [y_1(t) - y_2(t)] - [y_1(t - 2L_2/c) - y_2(t - 2L_1/c)] \quad (11)$$

where time delays have been adequately chosen to cancel out frequency noise effects. This is of course based on the fact that laser frequency fluctuations enter into  $y_1(t) - y_2(t)$  and into  $y_1(t - 2L_2/c) - y_2(t - 2L_1/c)$  with the same time dependence structure. Figure 5 shows a conceptual scheme of how this TDI variable cancels frequency noise.

There are many other TDI variables which cancel various noise components. The common philosophy is that they are generated by linear combinations of suitably time-shifted interferometer readouts.

### 3. *LISA*'s scientific objectives and requirements

The scientific objectives of *LISA* and the mission requirements are tightly bound together: there are noise constraints which limit what can be achieved in practice, and there are GW sources which one aims to see as best as possible. At the time of writing there is still debate within the *LIST* (*LISA* International Science Team [21]) on fine structure figures. Approximately, the sensitivity curve for *LISA* is shown in figure 6.

According to this curve, the strain sensitivity is  $\sim 7 \times 10^{-21} \text{ Hz}^{-1/2}$  at 3 mHz, where the noise minimum is located. Sensitivity worsens in a V-shaped curve as we move out of the trough in frequency domain. In terms of displacement noise, and taking into account that GW strain is a measure of *relative* distance changes,  $h = 2\delta L/L$  [3], the above is equivalent to  $S_L^{1/2} \simeq 20$  picometres/ $\sqrt{\text{Hz}}$  at 3 mHz.

As already stressed in the Introduction section, many and important GW sources are expected in *LISA*'s low frequency band. GW Sighting and characterisation of such sources are therefore

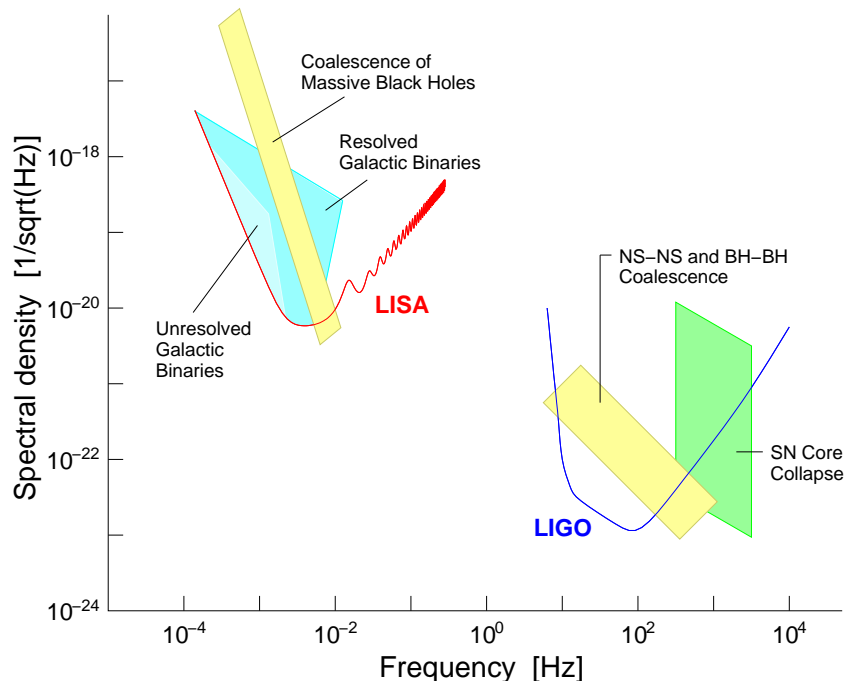


**Figure 6.** Spectral density of noise for *LISA*. Ground based *LIGO* sensitivity is also plotted for comparison. A few reference GW sources are quoted, too.

part of the mission’s scientific objectives. While objectives of this kind strongly rely on our belief that General Relativity is correct—in so far as we make *quantitative* estimates of GW intensities—, we may not forget that observations of the Universe through the *gravitational window* have never been made so far. So, when *LISA* gets operative, the unexpected should be expected. . . The GW Universe could well provide new fresh evidence that some of our current astrophysical and/or cosmological views need changes, or even hint at, or directly solve such difficult and paradoxical problems as modern Cosmology faces. By way of speculation, one may for example recall that 22% of the Universe is made of dark matter [22]; dark matter is not electromagnetically visible yet it does indeed gravitate—hence GWs could be generated there and bring information of this largely unknown form of matter.

There are three major areas of Physics where we can identify potential contributions by *LISA*. We list them below, along with some conjectured sources:

- (i) **Astronomy and Astrophysics:**
  - (a) Are Kerr black holes at the centre of active galactic nuclei?
  - (b) How do super-massive black holes form and grow?
  - (c) We can observe the evolution of thousands of galactic binaries
- (ii) **Cosmology:**
  - (a) How do super-massive black holes interact and contribute to the formation of galaxies?
  - (b) Study massive black holes up to redshifts of  $z = 30$
  - (c) Observe high redshift objects at gravitationally calibrated distances to more precisely determine the Hubble constant
  - (d) Independent measurements of dark energy parameters
- (iii) **Fundamental physics and discovery:**
  - (a) Test General Relativity at its *strong field* limit by mapping space-time near black holes
  - (b) Compare white dwarf binaries to theory (calibration binaries)
  - (c) Evidence of gravitational dynamics on cosmological scales:
    - Is there a first order phase transition at TeV scale energies?
    - Are there extra dimensions at the sub-millimeter scale?
    - Do cosmic superstrings exist?
  - (d) There will likely be so far unforeseen phenomena, unveiled by GW observations

To build hardware and software capable of implementing the requirements set forth in figure 6 is no mean feat, from the technology point of view. Actually, the technological road to *LISA* is by no means an easy one: the system is complex, and has many subsystems which will ultimately be integrated into a coherent whole. In fact in *LISA* the traditional division between spacecraft and payload cannot be clearly drawn: the payload takes continuous action on spacecraft navigation decisions, while the spacecraft computer continuously overviews and authorises actions by the payload computer.

#### 4. The *LISA* payload

We shall not delve into the detailed structure and assembly of the various parts of *LISA*. We shall however give a brief overview of its two most important subsystems—from the conceptual viewpoint—, i.e., the *drag free* and the Metrology subsystems.

##### 4.1. The *drag free* subsystem

Detection of GWs with *LISA*’s is only possible if the test masses follow nominally geodesic trajectories, i.e., those defined by the interplanetary gravitational field, *plus* the GWs themselves. These show up as time dependent gravity gradients which can be identified above an otherwise stationary background by certain specific signatures.

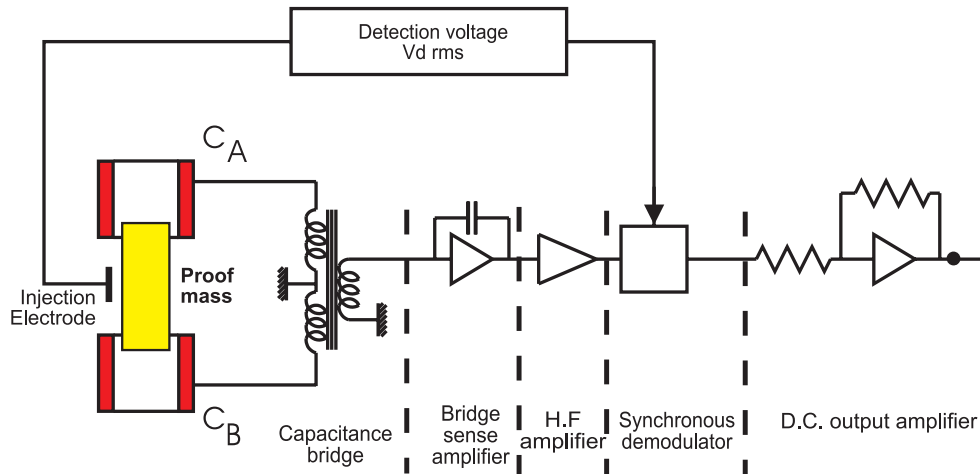


**Figure 7.** Scheme of the GRS capacitive sensing, only one channel.

A most delicate problem in *LISA* therefore is to make sure that the test masses do actually move along geodesics to *very high precision*. The problem to ensure this is that interplanetary space is in fact a considerably hostile medium: solar radiation pressure, ionising particle fluxes, and environmental magnetic fields are among the agents which would perturb geodesic motion should the test masses be floating *unshielded* in their orbits.

Apart from hosting the measuring and control instrumentation, the spacecraft play a fundamental role in providing the test masses adequate protection against external agents. Test masses are freely floating *inside* the spacecraft, and it is therefore the latter which receive the impact of perturbations, eventually being driven away from their geodesics. In order not to drag along the test masses with them, a so called *drag free* system is implemented in the satellites: this consists in a *gravitational reference sensor*, and an associated *actuation system*.

Each test mass is housed in a box whose walls are metallic plates which form capacitors with the faces of the test mass itself. In equilibrium conditions the mass is centred in the housing, and deviations thereof result in capacity changes, which are detected by corresponding bias voltage variations [23], see figure 7. This is called *gravitational reference sensor* (GRS). Its error signal is a voltage, proportional to the difference of the gaps on opposite sides of the test mass, and is used to send suitable ignition commands to a set of micro-thrusters which restore the centred positions of the test masses by acting on the spacecraft only. Micro-thrusters produce very gentle micro-newton forces by the ejection of ions, or atoms.

The electrode housing actually has several electrodes per face of the cubic test mass, whereby it can obtain and process full attitude control of the spacecraft —the so called DFACS, or Drag Free and Attitude Control System. The GRS, together with its complex electronics and control software, is a most essential part of *LISA*. In a system with so many degrees of freedom, and where *two* test masses are hosted in the same spacecraft, full implementation of the DFACS is not only subtle, it also requires eventual *back actuation* on the test masses by the GRS itself, though perpendicular to the corresponding interferometer arm.

#### 4.2. Optical Metrology System in *LISA*

The interferometry in *LISA* has some differences with that in earth based GW detectors. The latter are essentially Michelson. Apart from the already commented fact that *active mirrors* are needed in *LISA* to compensate for energy loss down the very long arm-length (with a small laser power of 1 watt), the system works in a three-stage scheme: first, the position of the test mass

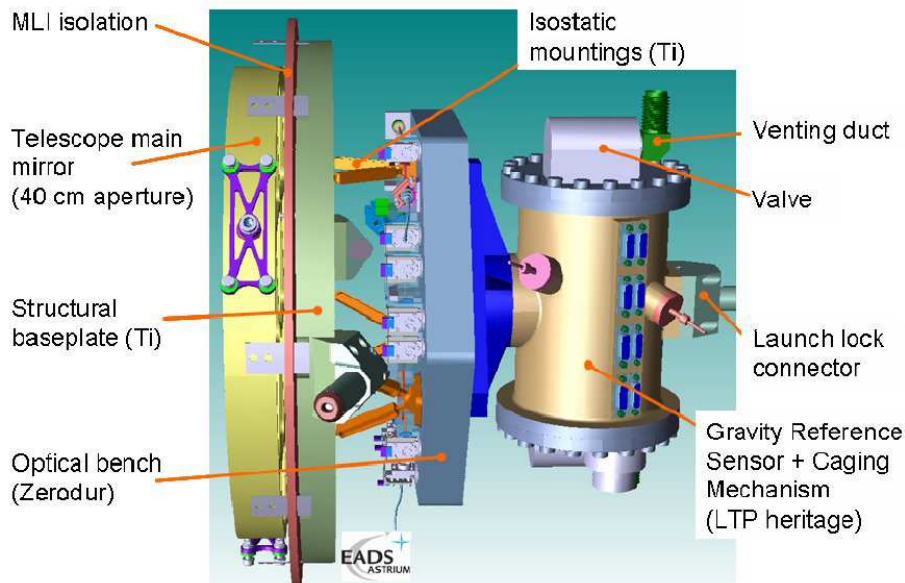


**Figure 8.** Mounting of the GRS on the Optical Bench. The telescope’s primary mirror is visible on the left. Thanks are due to Peter Gath and Ulrich Johann, from EADS-Astrium Friedrichshafen for providing this picture.

relative to the spacecraft is established; second, the distance between spacecraft is determined; and third, the position of the other end mass relative to its spacecraft is measured. A heterodyne operation mode is accepted in all cases [17].

The optical metrology consists of:

- The laser assembly, which includes the laser source proper, a Yag-Neodymium, 1 watt, 1.064 micron laser, plus the acousto-optical modulators (for heterodyning) and various stability and feedback controls. There is one per spacecraft (plus redundancy).
- The optical bench, which incorporates mirrors, beam splitters and photo-diodes for all the required interferometry modes. There is one per test mass, so two per spacecraft. No redundancy here.
- The telescope, which is a Cassegrain with a primary and a secondary mirror. The telescope collects the light coming from the remote spacecraft, and also re-emits it, sending the light in exactly opposite direction. There is one telescope per test mass, hence two per spacecraft. No redundancy, either.

Figure 8 represents a design view of the GRS mounting, together with its optical bench and telescope for a single test mass.

## 5. *LISA PathFinder*

The reader who has made it this far has surely acquired a flavour of the practical difficulties and challenges the *LISA* designers, engineers and even scientists have to face. Ultimately, it is all of course due to the extreme weakness of the GW signal we want to detect.

While the Science case to fly *LISA* is widely considered a strong one within the community, it is an obvious matter of course that the mission should only be launched when solid expectations that it will work are in place. In the space expert jargon, the question of *technology readiness* (or maturity) is the one which must be fixed before the mission gets full approval to take off.

Many of the technological capacities needed for *LISA* can be developed and tested on ground: an instrument which works in the laboratory can, in most cases, be tweaked in such a way that it will work in space, too. This requires the use of radiation-hard materials and electronic components, plus a number of structural and vibration tests which constitute the process known as *space qualification* procedure. Such process is very well established by space agencies, based on experience of about a half century of space flight, and resources to qualify a laboratory prototype according to the appropriate protocols are abundant in the specialised market.

But *LISA*'s *drag free* subsystem, which is the core of the mission, cannot be tested on earth: the extremely precise and long duration free fall conditions needed for a test of the GRS are simply orders of magnitude beyond the best gravity-free laboratory available on ground. In view of this, and in order to mitigate the risks of a direct launch of *LISA*, which is very expensive indeed, the European Space Agency (*ESA*) has decided to first fly a precursor mission where *LISA* technologies are put to test. The results of this mission will of course heavily bear on *LISA*'s timing and final design.

The precursor mission is called *LISA PathFinder* (*LPF*). It is part of *ESA*'s *SMART* (Small Missions for Advanced Research Technology) programme, of which it will be the *second* mission. *LPF* is scheduled to fly in 2009, and is now entering its industrial implementation phase, therefore a very advanced state of development. Seven European countries (voluntarily) participate in *LISA PathFinder*, which means national funding is provided in each case for the share of responsibility accepted by the corresponding party within the mission consortium. Specific national funding covers about 20% of the total mission cost, the rest being provided by *ESA*. The seven countries are: Italy, Germany, United Kingdom, Spain, Holland, Switzerland, and France.

The payload aboard *LPF* is the so called *LISA* Technology Package (*LTP*), whose details we shall come to shortly. The *LTP* is an entirely European instrument. However, given that *LISA* is conceived as a joint venture between *ESA* and *NASA*, it was long scheduled that *NASA* would provide their own version of the *LISA* precursor technology, to fly with the same space platform as the *LTP*. The American contribution was called Disturbance Reduction System (*DRS*). Unexpected difficulties during the development and test of the *DRS* have unfortunately led *NASA* to very significantly descope their contribution to the *PathFinder* test, which will now essentially consist of the *LTP*. *NASA* will however still provide a set of alternative micro-thrusters, together with software to drive them on the basis of data handed by the European Gravitational Reference Sensors.

In the following sections we describe the main parts and functionalities of *LPF* and the *LTP*, as well as their motivation and purposes.

## 6. *LPF* mission description

*LPF* will consist in a single spacecraft, hosting a pair of test masses. One of them acts as the GRS, while the other will be acted according to precisely defined operation modes. A laser interferometer will check that the level of *drag free* is the one required.

### 6.1. Orbit and general mission details

*LPF* will operate from the Earth-Sun Lagrange point *L1* —see figure 9, left. As we see indicated in the figure, *L1* is a *metastable* position, hence the spacecraft will actually revolve around it in a Lissajous orbit: this is a nearly circularly shaped trajectory in a plane which is almost perpendicular to the Sun-Earth line, see figure 9, right. Its diameter is almost 2 million kilometers, and it takes about 6 months to perform a complete rotation around it.

*LPF* will be launched in a *Rocket* vehicle, from the Russian space field at *Pliesietsk*, near *Arkangelisk* in Northeastern Russia. Launch date is currently fixed for the third quarter of 2009. The vehicle will be initially inserted into a slightly elliptic low Earth orbit, with an inclination

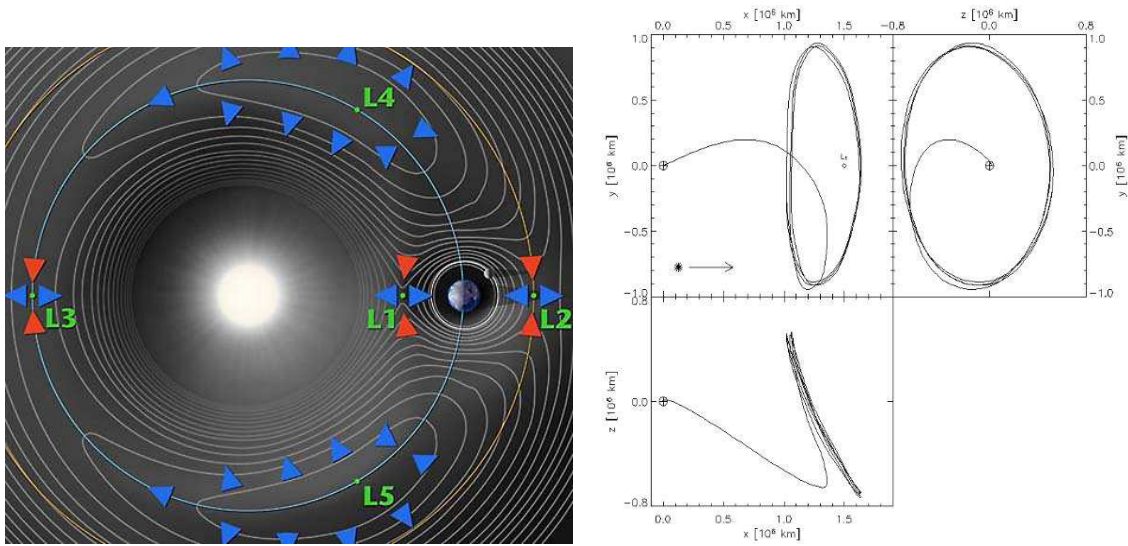


**Figure 9.** Left: the Lagrange points of the Earth-Sun system, and the gravitational field lines (the plot is *not* to scale). Right: Lissajous orbit for *LPF*, from the the three coordinate planes. Axes are labeled in millions of kilometres.

of  $63^\circ$ . The orientation of the line of apsides of the parking orbit must be adjusted to target for an operational orbit that fulfills the station visibility constraints, which is a minimum of 8 hours of visibility from the ground-station in Villafranca del Castillo, near Madrid (Spain). A sequence of between 11 and 15 manoeuvres will bring the spacecraft to a transfer towards *L1*, which is 1.5 million kilometres from Earth. In each manoeuvre, a speed increment of some 3 km/sec is applied to the spacecraft at the orbit's perigee. The new orbit after each thrust maintains the perigee altitude, while the apogee gets further away, thus progressively increasing the orbital eccentricity until the spacecraft gets eventually detached.

The trip time to operational orbit is some three months. The minimum mission lifetime is 200 days, with possible extensions if deemed necessary by the mission international consortium, and by *ESA*.

### 6.2. *LTP* concept and top level requirements

The *LPF* mission is intended to test in flight a number of essential parts of *LISA*, most notably the *drag free* subsystem, but also picometre interferometry in space and other subsystems and software. For that, a *LISA* arm is squeezed to 30 cm, as shown in figure 10.

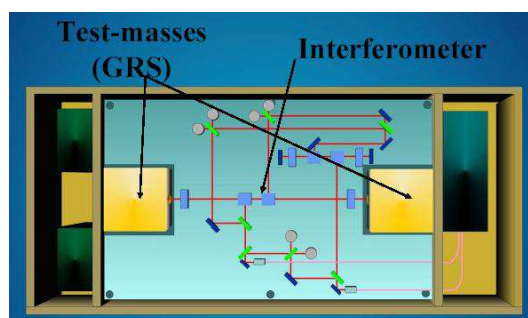


**Figure 10.** Conceptual diagramme of the *LTP*.

It has become common practice to convert GW noise spectral densities into *acceleration* noise spectral densities, which seems to be a more manageable concept from the experimentalist's point of view. To make the translation is however quite simple.

Let us first of all recall from the first paragraph of section 4.1 that GW effects show up as gravity gradients, or *tides*. Equivalently, by relative accelerations—hence forces—in the language of Classical Mechanics, or *geodesic deviations*, as General Relativity experts normally prefer. Taking as reference one of the test masses, the *relative* acceleration of the other is given by

$$\Delta a \equiv \frac{d^2 \Delta x}{dt^2} = \frac{L}{2} \frac{d^2 h}{dt^2} + \frac{\Delta F}{m} \quad (12)$$

where  $m$  is the mass of the second TM,  $\Delta x$  is the relative displacement,  $t$  is the quasi-Lorentzian time coordinate, and  $F$  embraces all non-gravitational forces, such as thermal, magnetic, electric, etc., and also non-inertial forces such as e.g. rotations. It is expedient to rewrite this expression in frequency domain:

$$\widetilde{\Delta a}(\omega) = -\omega^2 \widetilde{\Delta x}(\omega) = -\frac{L}{2} \omega^2 \widetilde{h}(\omega) + \frac{\widetilde{\Delta F}(\omega)}{m} \quad (13)$$

where a *tilde* ( $\sim$ ) stands for Fourier transform. If we now take spectral densities in the last equation we find, assuming of course that the true GW signal is deterministic, that the spurious forces  $\Delta F$  actually *fake* a GW noise with equivalent rms spectral density

$$S_h^{1/2}(\omega) = \frac{2S_{\Delta F}^{1/2}(\omega)}{mL\omega^2}, \quad \text{equivalent noise} \quad (14)$$

In terms of acceleration noise, the sensitivity requirement for *LISA* can be recast in the form

$$S_a^{1/2}(\omega) \leq 3 \times 10^{-15} \left[ 1 + \left( \frac{\omega/2\pi}{3 \text{ mHz}} \right)^2 \right] \frac{\text{m}}{\text{s}^2 \sqrt{\text{Hz}}}, \quad 0.1 \text{ mHz} \leq \frac{\omega}{2\pi} \leq 0.1 \text{ Hz}, \quad \text{LISA} \quad (15)$$

where the quadratic dependence on frequency here is simply because, according to equation (14), the acceleration noise can increase like  $\omega^2$  at high frequencies without affecting the GW sensitivity.

It has been agreed that performance of *LTP* can be considered fully satisfactory if the requirement for *LISA* is relaxed by one order of magnitude, both in spectral density of noise and in frequency band. More specifically [24],

$$S_a^{1/2}(\omega) \leq 3 \times 10^{-14} \left[ 1 + \left( \frac{\omega/2\pi}{3 \text{ mHz}} \right)^2 \right] \frac{\text{m}}{\text{s}^2 \sqrt{\text{Hz}}}, \quad 1 \text{ mHz} \leq \frac{\omega}{2\pi} \leq 30 \text{ mHz}, \quad \text{LTP} \quad (16)$$

The reason for this order of magnitude margin is this: if we could directly aim at *LISA*'s requirements then it would not make too much sense to fly a precursor mission, which costs time and money. On the other hand, the best *drag free* ever flown to date is several orders of magnitude less demanding than what we are requiring just for the *PathFinder*, so too big a jump might be unrealistic. If *LPF* returns satisfactory results, then we will have good hints on how to improve it so as to make it to *LISA*. We shall come back to this important issue.

### 6.3. Philosophy of the *LTP* test

The instrumentation and design of the *LTP* must ensure that any *residual accelerations*, i.e., those of unknown physical origin, be below the requirement expressed by equation (16). This requires in turn a detailed *apportioning* of different contributions to the background noise.

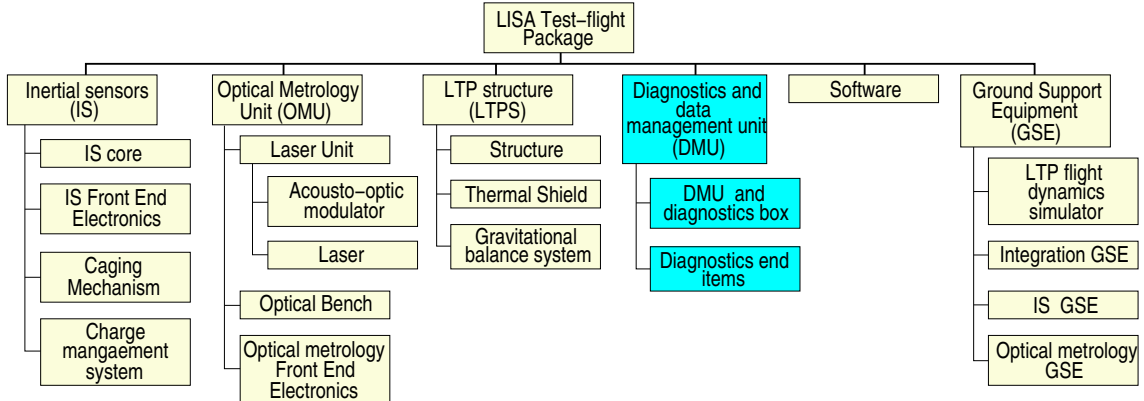


**Figure 11.** *LTP* functional diagramme scheme. Highlighted, the Spanish contribution.

An essential fact in this respect is the following: certain perturbing agents *couple* the spacecraft structure to the test masses, while others are independent of them. A sort of master equation can thus be set up:

$$a_{\text{noise}} = \frac{F_{\text{int}}}{m} + \omega_p^2 \underbrace{\left( x_n + \frac{F_{S/C}}{M\omega_{\text{fb}}^2} \right)}_{\substack{x_{S/C} = S/C \Leftrightarrow \text{TM} \\ \text{relative distance}}} \quad (17)$$

where  $F_{\text{int}}$  is the random force acting on a given test mass,  $\omega_p^2$  is the elastic constant (or *stiffness*) of coupling between the test mass and the spacecraft (can be a negative number),  $x_n$  is the random displacement fluctuations of the test mass and  $F_{S/C}$  the random force fluctuations acting on the spacecraft,  $\omega_{\text{fb}}^2$  is the elastic constant of the coupling between  $F_{S/C}$  and the test mass, related to the response time of the actuation system. Finally,  $M$  is the spacecraft mass, and  $m$  is the test mass mass.

All the parameters in (17) must be evaluated on the basis of experimental measurement, and to this end several measuring runs and operation modes have been designed [25]. In each case, the *LTP* interferometer will be used as a *diagnostic* instrument, as its foreseen sensitivity is already sufficient [26] to meet the measurement demands necessary to establish the validity of the limit set by equation (16).

#### 6.4. *LTP* functional architecture

It is most clearly explained graphically, as in figure 11, where all the *LTP* parts are ordered by function. We shall not attempt to give even a summary description of each subsystem here. We shall instead concentrate on the diagnostics and *DMU* subsystem, which is the highlighted branch of the drawing. Such will be the subject of the next sections.

### 7. The Data and Diagnostics Subsystem, or DDS

As shown in the highlighted branch of figure 11, it consists of two main parts: the Data Management Unit, or *DMU*, and the Diagnostics Elements. We first enumerate their components:

- (i) *DMU*. In spite of its name, it is the *LTP* computer. It is responsible for driving and control of the diagnostics items, and for such important tasks as the acquisition and on-board processing of phasemeter data. Some of these data are the mission science data. The *DMU*

also interfaces with other systems, in particular with the main mission computer —so called OBC (On Board Computer). The *DMU* has three main components, all of them *duplicated* as a resource against failure or malfunction. They are:

- (a) Power Distribution Unit (PDU)
  - (b) Data Acquisition Unit (DAU)
  - (c) Data Processing Unit (DPU)
- (ii) **Diagnostics Elements.** These are a number of sensors, plus their associated electronics, which are intended to monitor various disturbances happening inside the *LTP*. They are the following:
- (a) Precision temperature sensors. There are **22**, distributed across the *LTP*
  - (b) Calibration heaters. There are **14**, distributed in the GRS, the Optical Window and the suspension struts
  - (c) Precision magnetometers. There are **4** of *fluxgate* type, surrounding the *LTP*
  - (d) Calibration coils. There are **2**, one per GRS and both aligned with the line joining the test masses
  - (e) Radiation Monitor. There is just one, attached to the spacecraft’s shear walls.

Before going into any detail on the above, let us first discuss the relevance of the DDS for the *PathFinder* mission. While it is fairly obvious that the *DMU* is mission critical —i.e., if there is no *DMU* then there is no mission—, the reasons for the need of the Diagnostics Elements are less trivial yet fundamental for the real motivation of the *LPF*: to pave the way to jump across the sensitivity gap between *LPF* and *LISA*.

### 7.1. Why are the Diagnostics Elements crucial for *LPF*?

To answer this question, we first need to ask another question. Imagine *LPF* works perfectly, i.e., it proves to be compliant with the top level requirements expressed by equation (16) to exquisite precision. While this will likely bring to the *LPF* community a truly rewarding sense of achievement, a very important question will still remain open after such potential success. It is: “OK, but this an order of magnitude less sensitive than *LISA*; *how do we reach there?*”.

There are two tasks here: one is to identify which parts of the *LTP* are liable to sufficient improvement, the other to pursue suitable research to actually improve the system. The Diagnostics Elements constitute the essential tool for the first task, and can also be of great help for the second. Let us see now how this comes about.

Recall first of all that the *LTP* science readout is provided by the *phasemeter*, i.e., the interferometer output. There are several interferometry output channels —some of them for diagnostics, too—, but there is only one *science channel* proper. Relative accelerations can be easily translated into displacements (in Fourier domain there is just a  $-\omega^2$  factor between them), thence into phase shifts. The *LTP* phase readout is expected to be pure noise, no signals whatsoever (up to some serendipitous unpredictable discovery), with a spectral density at or below top level requirement values.

The problem we want to solve is to identify the magnitude of each of the various sources of noise which ultimately combine into the measured phase noise, where they add together entangled and undifferentiated. For this, we have the diagnostics elements.

Notice, however, that sensors alone are not sufficient: a question remains which is the relationship between, say, the temperature field across the *LTP* and the phase readout. To establish that relationship by theoretical analysis of the spacecraft structure is basically hopeless —there are too many parts: optical elements, flanges, screws, connectors, brackets, glass, harness,... It is more practical to resort to *in situ* measurements by a finite number of sensors, and to devise a procedure to generate controlled intense signals (for example thermal shocks), whose effect be clearly seen in the phasemeter. If temperature measurements are made

simultaneously with the shocks, the above procedure provides a way to establish the sought for relationship.

We can quantify the above. Let  $\phi(t)$  be the phase readout, which is a sampled time series. This total phase can be *apportioned* into various contributions —magnetic, thermal, laser phase noise, etc. Noting generically by  $\alpha$  any one of these, we can write

$$\tilde{\phi}(\omega) = \sum_{\alpha} \tilde{\phi}(\omega; \alpha) \quad (18)$$

where  $\tilde{\phi}(\omega; \alpha)$  is the contribution of the  $\alpha$  agent to the total  $\tilde{\phi}(\omega)$ , and where Fourier domain magnitudes have been used, as they are the ones which will be used in normal practice.

Our concern is the determination of the *feedthrough* coefficients

$$H(\omega; \alpha) = \frac{\partial \tilde{\phi}(\omega)}{\partial \alpha} = \frac{\partial \tilde{\phi}(\omega; \alpha)}{\partial \alpha} \quad (19)$$

In the linear regime, knowledge of the feedthrough coefficients suffices to calculate the contribution  $\tilde{\phi}(\omega; \alpha)$ :

$$\tilde{\phi}(\omega; \alpha) \simeq H(\omega; \alpha) \alpha \quad (20)$$

The problem therefore translates into how to actually measure  $H(\omega; \alpha)$ . The idea is to generate in the system such a strong  $\alpha$ -signal that the readout gets dominated by  $\tilde{\phi}(\omega; \alpha)$ . In this circumstance we have  $\tilde{\phi}(\omega) \simeq \tilde{\phi}(\omega; \alpha)$ , and hence a series of measurements of phase for various values of  $\alpha$  results in an estimate of  $H(\omega; \alpha)$ . Accuracy of the estimate is of course dependent on signal-to-noise ratio of the applied control signal. For the *LTP*, this is required to be 50 or larger [27].

Summing up, we *need* diagnostics sensors, plus suitable controlled perturbation generators, if we want to be able to focus future research activities towards *LISA*. Such is of course our ultimate motivation to build and fly *LPF*. We devote the following sections to review the research done so far on diagnostics elements for the *LTP*. *DMU* development will be left out, due reasons of space.

## 8. Thermal diagnostics

Temperature fluctuations are a source of disturbances in the *LTP*. Thermal gradient fluctuations cause pressure differences between test mass faces which tend to push them away from their centred position. This happens due to *radiometer* effect, *radiation pressure* effect, and *asymmetric outgassing*. In addition, temperature fluctuations do also affect the refractive index of optical elements in the optical bench, both due to temperature dependence of this quantity, and to stress induced dependence.

All in all, temperature fluctuations must be maintained below a certain level, otherwise the *LTP* readout noise will grow unacceptably high. Temperature fluctuation noise is not the only source of noise in the *LTP*, and a limit has been set to 10% of the top level requirement, equation (16). Analysis shows [28] that temperature fluctuations should be maintained at

$$S_T^{1/2}(\omega) \leq 10^{-4} \text{ K}/\sqrt{\text{Hz}}, \quad 1 \text{ mHz} \leq \omega/2\pi \leq 30 \text{ mHz} \quad (21)$$

This basic stability requirement sets the reference for thermal diagnostics, both for temperature sensor and calibration heaters performance.

### 8.1. Temperature sensing

The Industrial Architect is responsible to ensure that the spacecraft is able to maintain the *LTP* temperature conditions compliant with equation (21). If we are to measure temperature

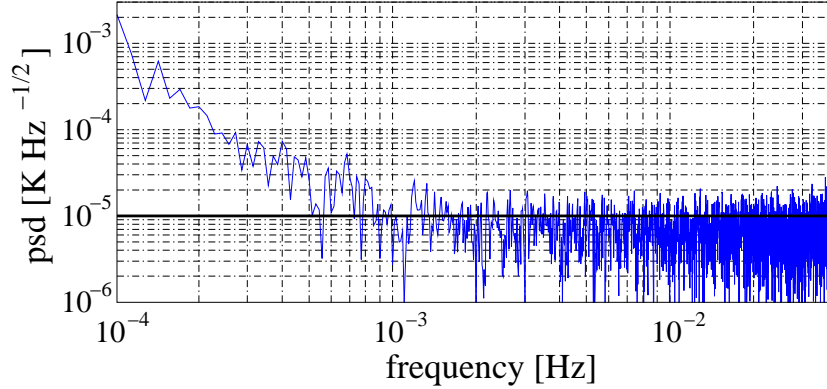


**Figure 12.** Spectral density data of NTC temperature sensors. Note full compliance with the requirement (22) throughout the measuring bandwidth.

fluctuations below that level, our sensing system must of course be less noisy. We have defined that one order of magnitude margin should be given to sensing, or

$$S_{T, \text{measurement}}^{1/2}(\omega) \leq 10^{-5} \text{ K}/\sqrt{\text{Hz}}, \quad 1 \text{ mHz} \leq \omega/2\pi \leq 30 \text{ mHz} \quad (22)$$

is the temperature sensing system requirement.

Suitable sensors can be either platinum resistors (PTD) or thermistors (NTC). *A posteriori*, the best choice has proved to be the latter [29]. Thermistors are electronic devices, hence conditioning circuitry is necessary to drive them and acquire their data. The requirement set by equation (22) is very demanding, indeed. A test of the instrumentation is accordingly difficult, since best laboratory thermal conditions are orders of magnitude less stable than (22). We have devised an insulating system which is capable to strongly screen ambient temperature fluctuations and generate an environment in its interior where thermal stability is 10 times higher than (21), and more.

Tests of the electronics and sensors are long duration. This is understood in terms of the large time constants of the insulator, but also because our measuring bandwidth (MBW) is around 1 mHz, hence periods in the order of hours. Many tests have been conducted in the last two years [28], with different sensors and setups, which have been used to constantly improve the performance of the temperature sensing system. Thermistors consistently gave one order of magnitude less noise than platinum resistors, and an example result is shown in figure 12.

## 8.2. Calibration heaters

As already explained, the key to using temperature sensors is to know their calibration properties. This is accomplished by means of heaters which generate suitable signals. The type of signals and the powers required for each set of heaters varies. We separately summarise the most relevant results.

**8.2.1. Inertial sensor heaters** A schematic diagramme is shown in figure 13, left: H1 through H4 are heaters, attached to the electrode housing. Colored rectangles labeled T1 through T4 are the electrodes, and T1, . . . , T4 their temperatures. To be noted that the heaters H1 and H3 form a *single logical heater*, which means they are driven at the same time by identical signals. The same applies to heaters H2 and H4.

GRS, or Inertial Sensor heaters activation scheme is shown in figure 13, right. It is actually required that both the period  $\tau$  and the *duty cycle* (ratio between the duration of the ON

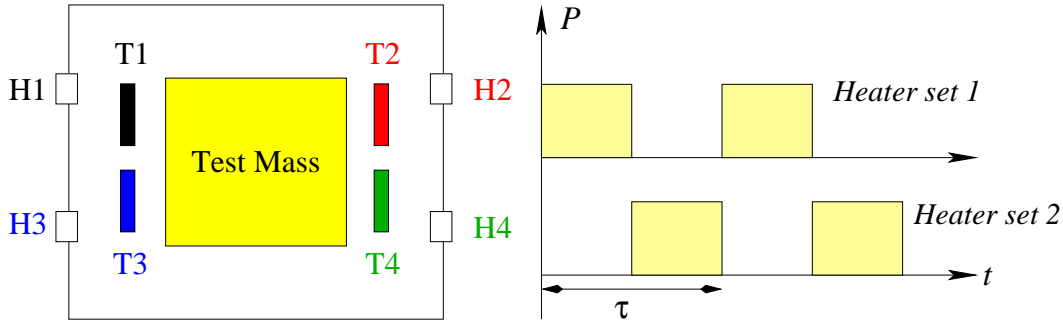
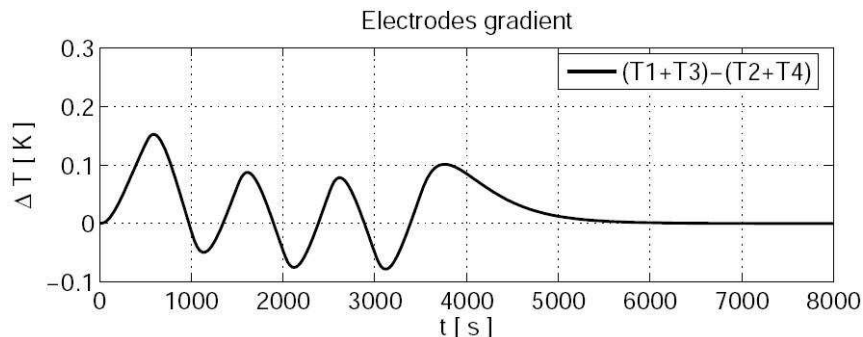


**Figure 13.** Heaters for the Inertial Sensor Heads (left) and their activation signals (right).

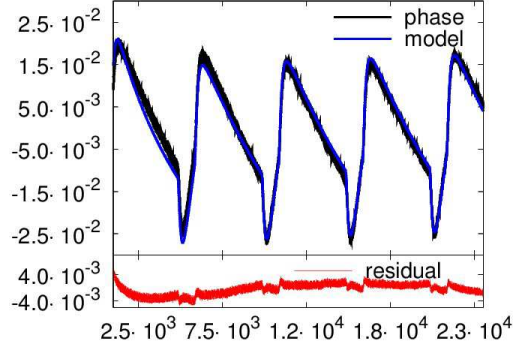
and OFF signal periods) be tunable by software. This ensures that the *LTP* bandwidth is scanned, which we need to fully characterise the system response. It is the Spanish DDS team's responsibility to define the optimum power and activation scheme for the *LTP* heaters. In the case of the ISH heaters this had to be done on the basis of simulation work, which is the only tool available at a time when the hardware is still under construction. Simulations are done with a software toolkit developed by *Carlo Gavazzi Space* (CGS) for the current *LTP* configuration.

Figure 14 is an example of simulation results, corresponding to  $\tau = 10^3$  seconds, duty cycle of 50% [30]. Imposing that signal-to-noise ratio be 50, the power of the heaters can be calculated. In this case, the CGS model indicates that 5 mW suffice. Similar methods applied to higher frequency signals show that powers are higher, as indeed expected. At the band's higher end, i.e., 30 mHz, 90 mW are needed. This is thus the requirement for ISH heaters' powers.

*8.2.2. Optical Window heaters* CGS's thermal model does not include the other important location for the placement of heaters: the optical windows (OW). Experiment has therefore been resorted to in order to properly characterise the OW response to heat shocks. To this end, a collaboration between Barcelona and Hannover was programmed to do an *in situ* series of measurements. The layout is seen in figure 15, left: the temperature sensors are four small black beads, two on the titanium and two on the glass. Heaters are less visible, as they are orange-colored kapton tapes, glued to the lateral surface of the titanium flange. Many data were gathered, and offline analysis is quite advanced. A good example is shown in figure 15, right.



**Figure 14.** Gradient response across the electrode housing for an alternate signal of 500+500 seconds.



**Figure 15.** The optical window, held in place on the titanium flange (left). On the right, a plot comparing phase data with a theoretical model.

The fit was done with a form of auto-regressive process [31]:

$$\phi(t) = \frac{a_1 + a_2 q^{-1}}{b_1 + b_2 q^{-1}} x(t) \quad (23)$$

where  $x(t)$  is some linear combination of the temperatures read by the sensors, and  $q$  is the shift operator:  $qx_n \equiv x_{n+1}$ ,  $q^{-1}x_n \equiv x_{n-1}$ .  $\phi(t)$  is the phase shift induced by the thermal signals (pulsed shocks) on the light going through the optical windows —determined by interferometry.

## 9. Magnetic diagnostics

The *LTP* test masses are two cubes 4.6 cm to the side, weighing 1.96 kg each. They are made of an alloy of gold and platinum with 70% Au + 30% Pt, which is a compromise between weak magnetic properties and mechanical resistance: magnetic-wise, 90% Au + 10% Pt would be better, but too high a ratio of gold would make the cubic block vulnerable to mechanical deformation during severe launch shocks.

To cast such an alloy is a process where ferromagnetic impurities can enter the alloy structure, thus leaving a remnant magnetic moment in the TM. Likewise, magnetic susceptibility will be present. State of the art measurement techniques for these magnitudes is the driver for a requirement on them, which is set to [24]:

$$|\chi| < 10^{-5}, \quad |\mathbf{m}_0| < 10^{-8} \text{ Am}^2 \quad (24)$$

With these magnetic properties, magnetic cleanliness requirements must be defined which ensure that no force and/or torque noise distorts the position of the test masses. Let us see how these requirements come about.

The magnetic force on a dipole of volume  $V$ , with roughly uniform magnetic susceptibility  $\chi$  and remnant magnetisation  $\mathbf{M}$ , is given by the textbook formula

$$\mathbf{F} = \left\langle \left[ \left( \mathbf{m}_0 + \frac{\chi V}{\mu_0} \mathbf{B} \right) \cdot \nabla \right] \mathbf{B} \right\rangle \quad (25)$$

where  $\langle \dots \rangle$  indicates space average over the volume of the test mass, and where  $\mathbf{m}_0 = \mathbf{M}V$ .

The important feature to stress here is the *quadratic* dependence of the force on the magnetic induction field  $\mathbf{B}$ , which is due to the susceptibility being different from zero, i.e., to the induced magnetic moment  $(\chi V/\mu_0) \mathbf{B}$ . The consequence of this is that magnetic force *fluctuations* also depend on DC values of the magnetic field. Requirements must accordingly be defined for *both* DC and fluctuating values of the magnetic field. Various compromises among different noise contributions result in the following table [24]:

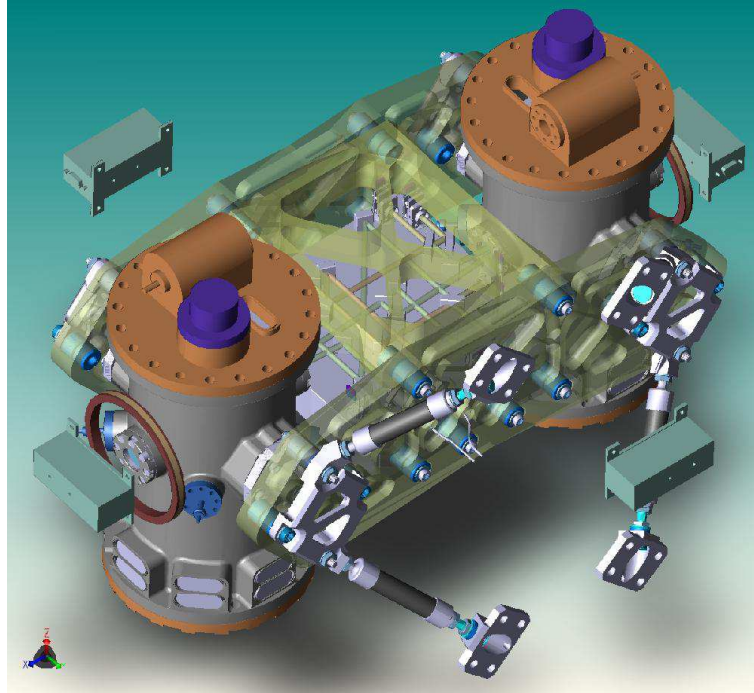


**Figure 16.** The external look of the *LTP*. Magnetometers and coils are drawn levitating to avoid obscuring the figure with the mechanical interfaces.

DC Magnetic field:	10	$\mu\text{T}$
DC Magnetic field gradient:	5	$\mu\text{T}/\text{m}$
Magnetic field fluctuations:	650	$\text{nT}/\sqrt{\text{Hz}}$
Magnetic field gradient fluctuations:	250	$(\text{nT}/\text{m})/\sqrt{\text{Hz}}$

The Industrial Architect must of course ensure that these requirements of magnetic cleanliness are met. As regards diagnostics, as already explained, the philosophy is different: we want to make magnetic measurements to gain as precise knowledge as possible of the values of all relevant magnetic magnitudes. We come to this now.

### 9.1. Magnetic field measurement

Magnetometers are often instruments based on high magnetic permeability cores which are submitted to saturation hysteresis cycles. These magnetic cores can severely challenge the magnetic cleanliness inside the *LTP*, and should therefore be kept safely away from the test masses. The most sensitive devices usable with the *LTP* are *fluxgate* magnetometers, which also have a magnetic core<sup>2</sup>. In addition, very sensitive fluxgates are usually heavy. All in all, we are forced to use only a few sensors, and far from the test masses. The consolidated requirement is that *four* be used, in a configuration which we see in figure 16. These constraints result in problems to create an accurate field map in the region where the test masses are, since an extrapolation of the magnetometers' readouts does not produce sufficient information, and (debatable) criteria must be applied on how to best make use of the available data.

Studies developed by us have provided an approach to address the problem of magnetic field extrapolation [32]. It is based on the datum that the sources of magnetic disturbance in the

<sup>2</sup> There are more sensitive devices, for example SQUIDS, but these require cryogenic conditions, hence cannot be possibly flown with the *LTP* due to unacceptable pump mechanical noise.

entire spacecraft are known, i.e., we know *where* they are, and their nominal *dipole moments*. What is of course unknown is their *fluctuations*. If all the magnetic dipole moments were actually known then one could reconstruct the magnetic field map by simple linear superposition of the fields of each dipole —but this of course does not happen in practice.

There are 51 identified sources, most of them PCBs (printed circuit boards), which means their magnetic dipoles are perpendicular to each board’s plane. This considerably reduces the number of unknowns, since knowing the 51 *moduli* of the dipole moment vectors suffices to completely identify them. This simplifies the problem, but we are still far from done: to determine 51 magnitudes from 12 experimental data is an under-determined, or *degenerate* problem: a multiply infinite set of solutions exists for it. The question is thus: can one solution be selected out of so many?

We have implemented a sort of least squares method for such selection, where random sets of solutions are iteratively compared, and a new selection is made in each step. The method is seen to converge, though final values have errors within up to 50 % of the real result. The analysis process is of course to be performed offline, and we are still working on improvements.

## 9.2. Magnetic coils

The purpose of the magnetic coils is to generate strong signals which cause forces to act on the TMs. Magnetic forces happen in non-uniform magnetic fields, so a single coil per TM has been selected for in-flight operations —this is the simplest scheme, see Figure 16.

Contrary to the situation with heaters, magnetic coils have an effect on the TMs which can be determined with high precision thanks to the well known laws magnetic induction by loop currents. This being the case, coils will be used to determine the magnetic properties of the TMs, which can later be used to calculate the magnetic noise contribution based on the magnetometers’ readings and the magnetic field evaluation described in the previous section.

Because of the quadratic dependence of the magnetic force on the magnetic field, the result of applying an oscillating current of well known frequency,  $\omega$ , to the coils is that the force acting on the TMs has two Fourier components: one at the same frequency  $\omega$  and one at double that frequency,  $2\omega$ . It is readily seen that

$$\mathbf{F}_\omega = (\mathbf{M} \cdot \nabla) \mathbf{B}_{\text{app}} + \frac{\chi V}{\mu_0} [(\mathbf{B}_{\text{ext}} \cdot \nabla) \mathbf{B}_{\text{app}} + (\mathbf{B}_{\text{app}} \cdot \nabla) \mathbf{B}_{\text{ext}}] \quad (26)$$

$$\mathbf{F}_{2\omega} = \frac{\chi V}{\mu_0} (\mathbf{B}_{\text{app}} \cdot \nabla) \mathbf{B}_{\text{app}} \quad (27)$$

where

$$\mathbf{B}_{\text{app}} = \mathbf{B}_0 e^{i\omega t} \quad (28)$$

is the applied field of the coils, and  $\mathbf{B}_{\text{ext}}$  is the otherwise prevailing field in the TMs.

Equation (27) shows that measurement of the system response at the double frequency,  $2\omega$ , suffices to determine the susceptibility of the test mass. To measure the remnant magnetisation  $\mathbf{M}$  is more complicated, as a *vector* measurement at frequency  $\omega$  needs to be done. Difficulties are however expected to be mitigated by previous on-ground measurements of these quantities, which should not be too affected by launch trauma.

The coils will be aligned with the line joining the test masses. They are 113 mm in diameter, 9 mm thick and are 81.5 mm away from the TMs. They have 2400 turns and will be fed by a current of a few milli-Amperes.

## 10. Radiation Monitor

Cosmic rays and certain solar events contain ionising particles which will hit the *LTP* in flight, thus causing spurious signals in the GRS. These particles are mostly protons, with 10 % or less

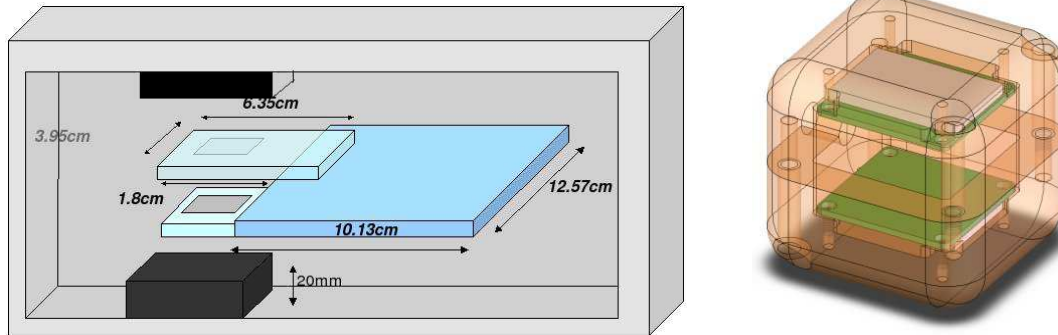


**Figure 17.** Radiation Monitor concept: two PIN diodes in telescopic configuration (left). The PIN diodes are shielded with a thick metallic layer (right).

of He nuclei, and a minor component of heavier galactic nuclei and solar ions. Charging rates and the properties of noise caused by charging vary depending on whether the particle flux comes from Galactic Cosmic Rays (*GCR*) or is augmented by Solar Energetic Particles (*SEP*). The reason is that the two types of radiation present different energy spectra, which result in different TM charging efficiencies. Temporal *fluctuations* of the *GCR* flux and *SEP* fake GW signals, and therefore a particle counter is necessary to provide correlations between the flux of energetic particles and the instantaneous charging rates observed in the test masses. The device must be able to determine the *energy spectra* of the detected particles, as this is the natural tool to tell *SEP* events from *GCRs*.

Not all charged particles hitting the satellite structure will make it to the test masses, as that structure itself has a certain *stopping power*. The particle counter must only be triggered by those particles having enough energy to reach the TMs, hence it must be properly *shielded*. Simulation work indicates that only ions with energies larger than  $\sim 100$  MeV should be counted [33]. The particle counter together with the above added capabilities is known as Radiation Monitor (RM).

The idea of the RM was first developed at Imperial College [34]. It is based on two PIN diodes, each of which can count individual particle hits. Photons are absorbed, while protons and heavier nuclei can exit through the opposite side of the diode. If placed in a telescopic configuration (see figure 17, left), the system can register coincidences and calculate spectra of the charged incident particles based on energy deposition in the PIN diodes. There is some degeneracy of course, due to the monitor's acceptance angle.

The actual implementation in hardware of these ideas has been carried through by a team at IFAE [35].

Contrary to the previous diagnostics, the RM does not require in-flight calibration. This is done on ground by submitting it to laboratory proton beam irradiation. An experiment was prepared in the Paul Scherrer Institute (PSI, Switzerland) in November 2005 to check that the shield was working as expected —previous tests of the electronics had of course been done earlier. An example result is shown in figure 18, which shows very satisfactory confirmation that simulation predictions were correct. To obtain such results was however not immediately straightforward, as various simulation and hardware parameters had to be properly tuned to give proper account of a number of non-obvious experimental facts [36].

An unexpected potential complication emerged out of the November 2005 proton beam run: evidence was found that, under heavy proton flux exposure (up to  $\sim 10^{10}$  protons), copper gets activated. A new PSI run was set up in November 2006. Final conclusions are still pending at the time of writing. We do not expect major RM shield changes to be required, but the results of the analysis will be necessary for a thorough understanding of the RM readout.

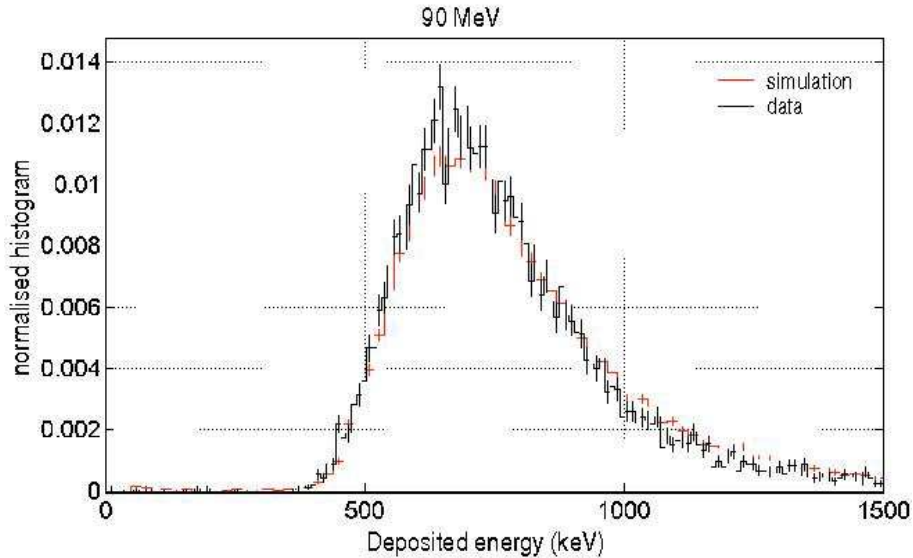


**Figure 18.** Comparison of deposited energy spectra from simulation (red) and test beam data (black) for 90 MeV protons.

## 11. Conclusion

The history of GW detection science is almost 50 years old. The long striven for detection has not been successful yet, despite the life long efforts of already two generations of researchers world wide. The reward to these people, and their funding bodies, has surely been the confirmation of truly impressive progress in instrument sensitivity. Laboratory detectors have limitations bound to their being on the Earth surface, and this constrains their viability to GW signals with spectra in the kHz band. *LISA* will be free from such limitations by going to outer space, thence making observations at much lower frequencies, in the milli-Hz band. Even if, as we expect, Earth detectors see GW signals well before *LISA* flies, this joint *ESA-NASA* mission will be a unique GW observatory, specific to the low frequency spectrum.

*LISA* is of course a complicated mission. Even though its scientific case is almost universally acknowledged, the difficulties of its implementation initially caused numerous caveats about its real viability. Nevertheless enthusiasm for *LISA* has mounted internationally in the last five years or so: the community is now well organised into working groups, and the number of papers on *LISA* has soared. But no less engineering activities are thriving, too, as the precursor *LISA PathFinder* approaches its definitive implementation stages. *LPF* successfully completed its Preliminary Design Review (PDR), and is now going through Critical Design Review (CDR), the last stage before full speed manufacture begins. Current plans schedule *LPF* launch for late 2009, and indications are positive about feasibility. The challenge will then be the analysis of the mission results, which will be crucial for *LISA*. We have good hopes that success will come, and this paper intends to contribute evidence that such hopes are based on reason, not on wishful thinking.

## Acknowledgments

We thank the Spanish *Ministerio de Educación y Ciencia* for support, contract ESP2004-01647.

## References

- [1] Einstein A and Davis F A 1952 *The Principle of Relativity* (Newy, NY: Dover)
- [2] Pais A 1982 *Subtle is the Lord —the Science and the Life of Albert Einstein* (Oxford: Clarendon)
- [3] Weinberg S 1972 *Gravitation and Cosmology: Principles and Applications of the General Theory of Relativity* (New York, NY: Wiley & Sons)
- [4] Landau L D and Lifshitz E M 1985 *The Classical Theory of Fields* (Oxford: Pergamon)
- [5] Thorne K S 1980 *Rev Mod Phys* **52** 299
- [6] Weisberg J M and Taylor J H 2004 *Proc. 2004 Winter Conference on Astrophysics (Aspen)* ASP Conf. Series vol 328, ed F A Rasio and I H Stairs (Provo, UT: Astronomical Society of the Pacific) p 25
- [7] Weber J 1969 *Phys Rev Lett* **22** 1320
- [8] Astone P *et al* 2006 *Class Quant Grav* **23** S169
- [9] Baggio L *et al* 2005 *Phys Rev Lett* **95** 081103
- [10] Drever R W P 1983 *Gravitational radiation* ed N Deruelle and T Piran (Amsterdam: North Holland) p 321
- [11] D Sigg, *Status of the LIGO detectors*, *Class Quant Grav* **23**, S51S56 (2006)
- [12] Braccini S *et al* 2005 *Astropart Phys* **23** 557
- [13] Hewitson M 2004 *Class Quant Grav* **21** S1711
- [14] Fritschel P 2003 *Proc. SPIE Conference on Astronomical Telescopes and Instrumentations (Waikoloa, HI)* Proceedings of SPIE Vol. 4856, ed M Cruise and P Saulson (Bellingham, WA: SPIE) p 282. Also, [gr-qc/0308090](http://gr-qc/0308090)
- [15] See *LISA* webpages at <http://sci.esa.int/science-e/www/object/index.cfm?fobjectid=39174> and <http://lisa.jpl.nasa.gov>
- [16] Lobo J A 1992 *Class Quant Grav* **9** 1385
- [17] A Hammesfahr *et al* 2000 *LISA Final Technical Report ESTEC* Contract no. 13631/99/NL/MS Report no LI-RP-DS-009
- [18] Folkner W M, Hechler F, Sweetser T H, Vincent M A and Bender P L 1997 *Class Quant Grav* **14** 1405
- [19] Bender P L 1990 (unpublished notes)
- [20] Tinto M and Dhurandhar S V 2005 *Living Rev Rel* **8** 4
- [21] <http://www.srl.caltech.edu/lisa/index.html>
- [22] Bennett C L *et al* 2003 *Astroph J Suppl* **148**, 1
- [23] Carbone L, Cavalleri A, Dolesi R, Hoyle C D, Hueller M, Vitale S and Weber W J 2003 *Phys Rev Lett* **91** 151101 (2003). *Ibid.* 179903
- [24] Vitale S *et al* 2005 *Science Requirements and Top-level Architecture Definition for the Lisa Test-flight Package (LTP) on Board LISA PathFinder (SMART-2)* doc code LTPA-UTN-ScRD-Iss003-Rev1 (Trento: University of Trento)
- [25] Vitale S *et al* 2006 *LISA Pathfinder Experiments Master Plan*, ESTEC doc code S2-EST-PL-5007 (Noordwijk, H: ESA)
- [26] Heinzl G *et al* 2004 *Class Quant Grav* **21** S581
- [27] Lobo J A 2005 *DDS Science Requirements Document IEEC* doc code S2-IEEC-RS-3002 (Barcelona: IEEC)
- [28] Lobo J A, Nofrarias M, Ramos-Castro J and Sanjuan J 2006 *Class Quant Grav* **23** 5177
- [29] Ramos-Castro J and Sanjuan J 2005 *Temperature Sensors and FEE Prototype Test IEEC* doc code S2-IEEC-TR-3001 (Barcelona: IEEC)
- [30] Nofrarias M 2006 *DDS heaters characterisation IEEC* doc code S2-IEC-TN-3025 (Barcelona: IEEC)
- [31] Nofrarias M *et al* 2006 *Proc. 6th International LISA Symposium (Greenbelt, MD)* AIP Conference Proceedings vol 873, ed S M Merkowitz and J C Livas (Melville, NY: Springer) p 199
- [32] Martínez L and García S 2006 *Reconstruction of the Magnetic Field and Gradient on Test Masses of LISA PathFinder*, IEEC document code S2-IEEC-TN-3024 (Barcelona: IEEC)
- [33] Araújo H M, Wass P, Shaul D, Rochester G and Sumner T J 2005 *Astropart Phys* **22** 451
- [34] Araújo H M and Wass P 2005 *Simulations of the LISA PathFinder Radiation Monitor Performance*, ICL doc code S2-ICL-TN-3004 (London: ICL)
- [35] Boatella C and Puigdengoles C 2005 *LISA PathFinder Radiation Monitor Prototype Design*, IFAE doc code S2-IFAE-DDD-3002 (Barcelona: IFAE)
- [36] Wass P 2006 *Radiation Monitor test at PSI*, IEEC doc code S2-IEC-TR-3005 (Barcelona: IEEC)